THE JOURNAL OF PHYSICAL CHEMISTRY Letters

LETTER

pubs.acs.org/JPCL

Characterization and Application of Surface Plasmon-Enhanced Optical Diffraction from Electrodeposited Gold Nanowire Arrays

Ying Han and Robert M. Corn*

Department of Chemistry, University of California-Irvine, Irvine, California 92697, United States

ABSTRACT: Arrays of gold nanowires formed by the process of lithographically patterned nanowire electrodeposition (LPNE) were characterized by a combination of SEM, polarized UV−visible absorption spectroscopy, and optical diffraction measurements. A transverse localized surface plasmon resonance (LSPR) was observed for gold nanowire arrays with an absorption maximum (λ_{max}) that varied with nanowire width. Transmission optical diffraction measurements were measured with the even and odd diffraction orders creating an alternating, out-of-phase sinusoidal intensity pattern characteristic of the LPNE nanowire arrays. The intensities of the even diffraction order maxima were the strongest for nanowires with a width of 115 ± 10 nm; nanowires of this width exhibit a λ_{max} of 635 ± 10 nm, verifying that the transverse LSPR has enhanced the optical diffraction signal. Real-time total internal reflection diffraction intensity measurements were used to monitor in situ the electrodeposition of silver monolayers onto the gold nanowire arrays.

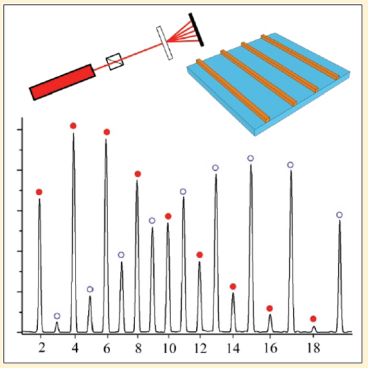

SECTION: Nanoparticles and Nanostructures

Nanostructured materials with high aspect ratios such as nanorods, nanowires, and nanoline patterns often exhibit anisotropic electronic and optical properties that differ from those observed in the bulk materials. These unique materials can be used to create many interesting devices, including sensitive chemical and biochemical sensors.[1−7] We have recently analyzed the optical diffraction at 633 nm from gold nanowire arrays on glass substrates that were created using the electrochemical fabrication methodology of "lithographically patterned nanowire electrodeposition" (LPNE) developed by Penner et al.[8−10] The gold nanowires in these arrays are spaced by approximately 5−10 μm and have widths and heights that can be varied independently from 15 to 500 nm. The optical diffraction from these nanowire arrays at visible wavelengths can span up to 60 diffraction orders and always present a unique diffraction pattern with separate oscillating intensities for the even and odd-order diffraction order intensities that is directly related to the array spacing structure.[11]

In this Letter, we show that these LPNE gold nanowire arrays can support a transverse localized surface plasmon resonance (LSPR), whose resonant wavelength depends on the width and height of the nanowires.[12−15] Transverse LSPRs have been previously observed on nanowire arrays: for example, Schider et al. have reported an LSPR in the UV−vis absorption spectrum of nanowire arrays created with e-beam lithography.[12] Through the combination of polarized UV−vis absorption spectroscopy, scanning electron microscopy (SEM), and optical diffraction measurements, we show here that LPNE gold nanowire arrays also exhibit a transverse LSPR absorption band at optical wavelengths and that the optical diffraction from the nanowire arrays is enhanced when the laser wavelength coincides with the maximum wavelength for the LSPR absorption. We denote diffraction at this resonant wavelength as "surface plasmon-enhanced optical diffraction." As a first demonstration of the utility of these optical diffraction measurements, we use the plasmon-enhanced optical diffraction signal to monitor in situ the electrochemical deposition of silver monolayers onto the gold nanowire arrays.

A series of LPNE gold nanowire arrays were created on BK7 glass substrates for the UV−vis and diffraction measurements. The LPNE fabrication process was implemented as previously described, starting with a master grating pattern of 7.5 μm spacing to create nanowire arrays of the dimensions shown schematically in Figure 1a. The length (L) of the nanowires was ∼1 cm and the height (h) of nanowires in these arrays was fixed at 30 nm by the thickness of the vapor-deposited sacrificial nickel thin film. The average width (w) of the nanowires was the same for all nanowires in a given array and was varied from 45 to 140 nm by controlling the gold electrodeposition time. The widths and spacings of the nanowire arrays were all measured with SEM; an example of a SEM nanowire width measurement is also shown in Figure 1. The average spacing between the nanowires for all samples was ∼7.5 μm, but as shown in the Figure, the exact spacing in the LPNE nanowire arrays was an alternating pattern of $D + \Delta$ and $D - \Delta$ where the asymmetry parameter Δ was a function of the etching time and nanowire width[11] and varied from sample to sample in the range of 70 to 200 nm.

Polarized UV−visible absorption spectra were obtained from this series of LPNE gold nanowire arrays; representative absorption spectra are shown in Figure 1b for four different arrays with nanowire widths of 58, 75, 108, and 140 nm. As seen in the

Received: May 18, 2011
Accepted: June 10, 2011

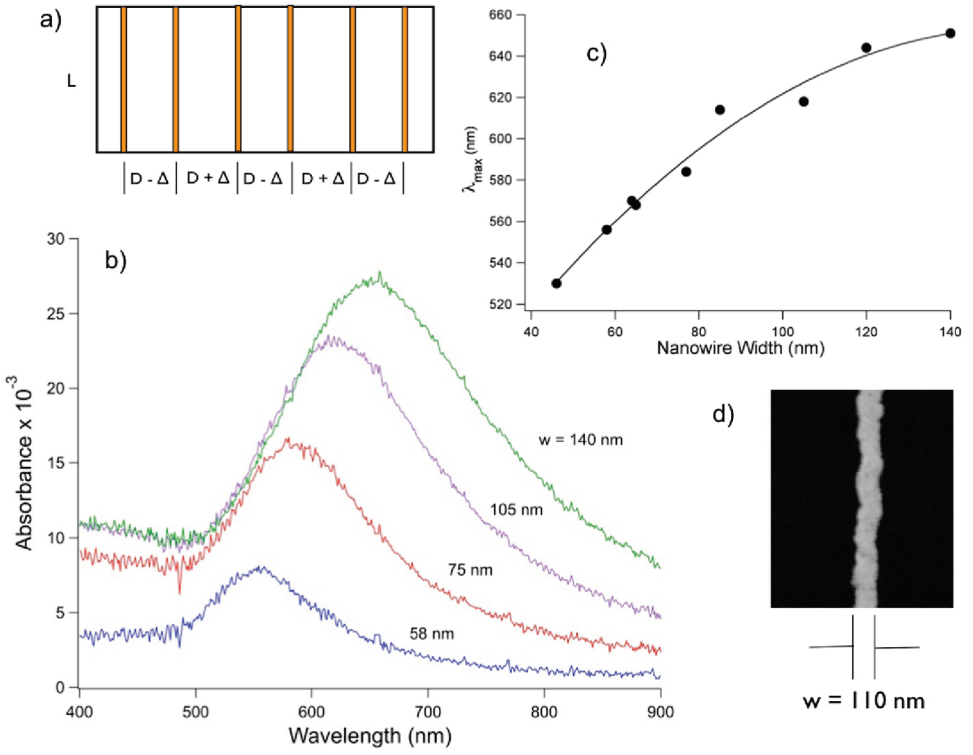

Figure 1. (a) Schematic diagram of LPNE gold nanowire array: L = 1 cm, D = 7.5 μm, Δ = 200−300 nm. (b) Polarized UV−vis spectra of four LPNE gold nanowire arrays with various widths (w = 58, 75, 105, 140 nm) on BK7 glass substrates. Polarization of the light was perpendicular to the nanowire long axes. Height of the gold nanowires was 30 nm. (c) Absorption maxima (λ_{max}) in the polarized UV−vis spectra of LPNE gold nanowire arrays as a function of nanowire width, w. (d) SEM image of a typical nanowire in a LPNE gold nanowire array (w = 110 nm; h = 30 nm).

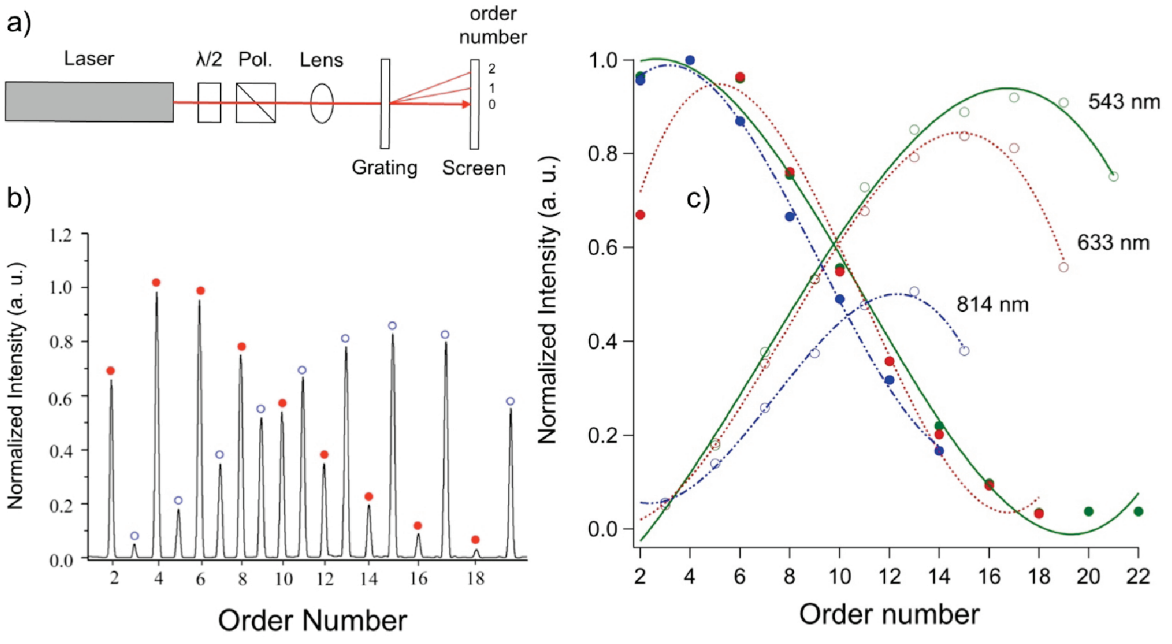

Figure 2. (a) Schematic diagram of transmission geometry used to obtain diffraction spectra. A $\lambda/2$ plate and a polarizer were used to control the intensity and final polarization. (b) Transmission diffraction spectrum of an LPNE gold nanowire array at 633 nm. Width w = 75 nm, h = 30 nm, D = 7.5 μm, Δ = 130 nm. Circles: even orders; squares: odd orders. (c) Relative intensities of the even and odd diffraction orders for the nanowire array at 543 (green circles, solid lines), 633 (red circles, dotted lines), and 814 nm (blue circles, dashed lines).

Figure, an absorption band was observed for all of the nanowire arrays with an absorption maximum (λ_{max}) and overall intensity that increased with nanowire width. This absorption band was only observed when the incident light was polarized perpendicular

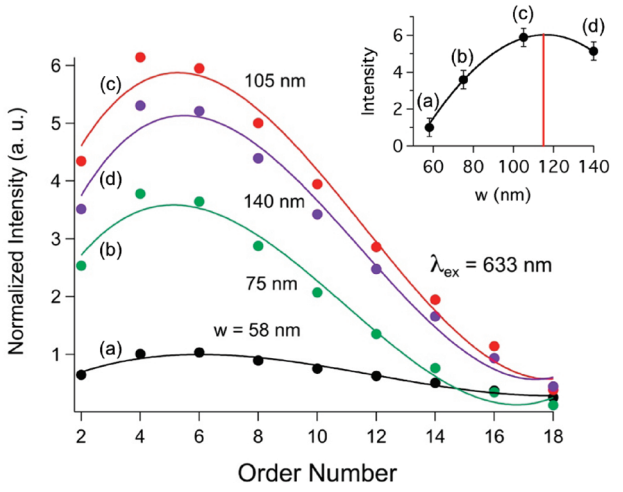

Figure 3. Relative diffraction intensity at 633 nm of the even diffraction orders for four LPNE gold nanowire arrays with different widths: (a) 58 (λ_{max}: 556 nm), (b) 75 (λ_{max}: 584 nm), (c) 105 (λ_{max}: 620 nm), and (d) 140 nm (λ_{max}: 655 nm). The inset plots the maximum relative diffraction intensity for these four arrays as a function of nanowire width. The solid curve is a quadratic fit to the data, which predicts that the largest maximum relative diffraction intensity should occur for nanowires with a width w = 115 nm.

to the long axes of the nanowires; we attribute this absorption to a nanowire transverse LSPR. Figure 1c plots λ_{max} as a function of nanowire width, which increases monotonically from w = 45 to 140 nm. The systematic increase in λ_{max} with increased width has been previously observed for both gold nanowires[12] and gold nanorods.[16,17]

In conjunction with the absorption spectra, optical diffraction data were obtained from these nanowire arrays at 543, 633, and 814 nm using the transmission geometry depicted schematically in Figure 2a. A typical LPNE nanowire array diffraction intensity pattern is shown in Figure 2b for a nanowire array with nanowires of width w = 75 nm. The array had an alternating wire spacing with D = 7.5 μm and an asymmetry Δ = 130 nm. The diffraction orders are labeled by their order number m as determined from the grating equation. (See Figure 2a.)[11] The even-order modes in the diffraction pattern are labeled with the solid red circles, and the odd-order modes are labeled with the open blue circles. As previously observed, the intensities of the diffraction orders from the LPNE nanowire array show a pronounced alternating intensity pattern of two out-of-phase sinusoidal patterns for the even- and odd-order diffraction modes due to the alternating nanowire spacing in the array ($D \pm \Delta$).[11] The even and the odd intensity maxima patterns can be fit with w, D, and Δ using a simple FT convolution theory developed in our previous paper.[11] Figure 2c shows the relative diffraction intensity for this grating at the three different wavelengths. The maximum relative intensity of the even and odd orders was found to be most similar at 543 nm, decreasing monotonically at longer wavelengths. We attribute this decrease to the amount of mismatch between the diffraction wavelength and the asymmetry parameter Δ.[11]

Figure 3 shows the relative intensities of only the even diffraction orders plotted versus order number obtained from transmission geometry diffraction experiments from the four nanowire arrays used for Figure 1b (w = 58, 75, 108, 140 nm). The even-order relative intensity patterns were each fit with a four-parameter polynomial regression (the solid lines in the Figure); the maximum relative intensities of these fits all occur between orders 4 and 6. These maxima are plotted in the inset of the Figure 3 as a function of nanowire thickness. The four points in the inset were fit with a parabolic curve (the solid line) that has a maximum at a nanowire width of 115 $\pm$ 10 nm, which is approximately six times the intensity of the diffraction from 58 nm nanowires. If we refer back to Figure 1c, then we see that this nanowire width corresponds to nanowire arrays with a transverse LSPR absorption maximum of 635 $\pm$ 10 nm, exactly coincident with the 633 nm laser wavelength. We therefore conclude that the optical diffraction from these nanowire arrays is enhanced by the presence of the transverse LSPR, and we denote this effect as "surface plasmon-enhanced optical diffraction". A number of research groups have previously observed surface plasmon-enhanced optical diffraction from gold gratings with micrometer widths and also from gratings decorated with gold nanoparticles.[18−31] The enhancement of diffraction intensity for a given nanowire width/wavelength combination observed for the LPNE nanowire arrays is directly related to the transverse LSPR of the nanowires; this resonance can be easily tuned to a different wavelength by varying the nanowire width in the LPNE process.

As a first demonstration of the utility of these optical diffraction measurements, changes in the diffraction intensity from LPNE gold nanowire arrays were used to monitor in real time the electrodeposition of silver onto the nanowires. Silver, of course, is an excellent plasmonic material, and coating the gold nanowires with a thin film of silver should increase the diffraction efficiency of the nanowire array. The nanowire array electrodes (for these experiments, nanowire arrays were created with dimensions h = 50 nm, w = 80 nm, D = 7.50 μm, Δ = 70 nm) were attached to an SF10 substrate (and an SF10 prism via index-matching fluid) to create a total internal reflection (TIR) geometry for the optical diffraction measurements. The nanowire array was also in contact with an aqueous solution and served as the working electrode in a three-electrode potentiostatic electrochemical cell; the combined optical-electrochemical cell used in these measurements is shown in Figure 4a.

Real-time in situ optical diffraction data (signal from a photodiode positioned on order number m = 2) and electrochemical data (cyclic voltammograms, CVs) were obtained simultaneously from the gold nanowire arrays. Figure 4b,c plots, respectively, the CV and the diffraction intensity signal observed during the electrodeposition of silver onto the gold nanowire arrays. The electrode potential was first swept cathodically from 0.9 to 0.3 V versus Ag/AgCl and then back anodically from 0.9 to 0.3 V. The cathodic current shown in Figure 4b that starts at ~0.4 V during the cathodic scan is due to the electrodeposition of silver onto the gold nanowires. This electrodeposition is observed throughout the rest of the cathodic scan and then continues during the anodic scan until the electrode potential again reaches 0.4 V. An integration of the cathodic current resulted in an electrodeposited charge corresponding to approximately six Ag monolayers. The diffraction intensity obtained simultaneously with the CV is plotted in Figure 4c; the diffraction signal increased at all potentials below 0.4 V during the electrodeposition of silver, on both the cathodic sweep (black line) and the anodic sweep (red line). The increase in the nanowire diffraction signal due to the electrodeposition of silver is attributed to the excellent plasmonic properties of the metal. Specifically, silver thin films support surface plasmon polaritons at optical wavelengths; in fact, the optical properties of the silver are slightly better than

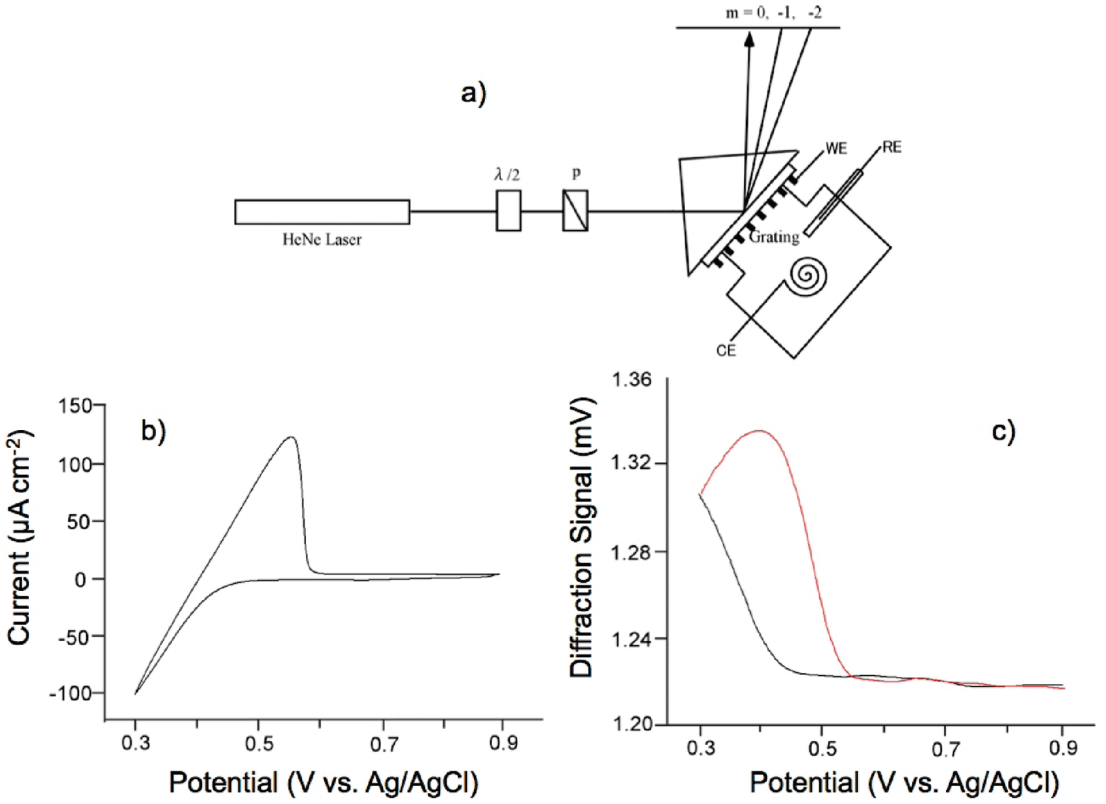

Figure 4. (a) Schematic diagram of the in situ diffraction experiment for gold LPNE nanowire arrays in an electrochemical cell. An SF10 prism is used in these experiments, and the diffraction is measured in a total internal reflection (TIR) geometry with the laser incident at the SF10-water critical angle of 50.6°. (b) Cyclic voltammogram (CV) for electrochemical deposition of silver onto the LPNE gold nanowire array (w = 80 nm, h = 50 nm, L = 1 cm, 1000 nanowires) in 20 uM Ag_2SO_4 + 0.1 M H_2SO_4 solution. Integration of the current density results in a total charge corresponding to approximately 6 monolayers of electrodeposited silver. (c) 633 nm optical diffraction signal obtained during the CV from the m = 2 diffraction order in the TIR geometry. The red portion of the plotted curve is the diffraction signal observed on the return (anodic) sweep of the CV.

those of gold at 633 nm (n_{Ag} = 0.1346 + 3.988i and n_{Au} = 0.1726 + 3.4218i).[32] These superior optical properties lead to sharper SPR resonances and longer surface plasmon propagation wavelengths for silver versus gold thin films at 633 nm. At potentials above 0.4 V on the anodic scan, the diffraction signal decreased as the silver was removed from the surface. At the end of the anodic scan, the diffraction signal returned to its original value, showing the reversible nature of this nanowire electrodeposition process. It is evident from the diffraction signals observed in this experiment that the surface plasmon-enhanced optical diffraction signal has submonolayer sensitivity for the detection of silver atoms on the gold surface.

In summary, in this Letter, we have characterized the surface plasmon-enhanced diffraction from LPNE gold nanowire arrays at optical wavelengths due to the presence of a transverse LSPR absorption in the gold nanowires. At 633 nm, maximum diffraction intensity patterns were obtained with gold nanowires of 115 nm in width; we found that this width also was the nanowire width required to create a λ_{max} at 635 nm in the transverse LSPR absorption spectrum. Additional measurements demonstrated that these diffraction intensities are very sensitive to changes such as silver electrodeposition onto the gold nanowire arrays. The LPNE process is a very convenient method for creating metal nanowire arrays of variable height and width over large areas (square centimeters), and we expect that the optical diffraction methods employed here will be a very convenient method of monitoring various nanowire surface adsorption processes. Future experiments will focus on the detection of molecular adsorption processes onto the LPNE gold nanowire arrays with optical diffraction measurements at various wavelengths for sensor applications.

EXPERIMENTAL METHODS

Grating Fabrication and SEM Measurements. Gold nanowire arrays were fabricated on 18 mm × 18 mm BK7 and SF10 glass substrates (Schott Glass) using the LPNE technique described previously.[11] Arrays of ~1500 nanowires were fabricated with an average internanowire spacing of D = 7.5 μm. The exact spacing between nanowires was in an alternating pattern $D + \Delta$: $D - \Delta$: $D + \Delta$: D − Δ, where the asymmetry parameter Δ depended on both the etching time and nanowire width.[11] The height (h) of the gold nanowires was determined by the initial Ni thin film deposition and was 30 nm for the BK7 substrates used in the transmission diffraction experiments and 50 nm for the SF10 substrates used in the diffraction measurements in the in situ TIR electrochemical cell. The width (w) of the nanowires was varied from sample to sample from 45 to 130 nm. Exact values of D, Δ, and w were obtained from SEM images taken on a FEI/Philips XL-30 FEG at 10 keV. Prior to imaging, the nanowire array samples were sputter-coated with a 1 to 2 nm of gold Au to minimize charging effects.

Polarized UV−vis Absorption Measurements. Polarized UV−visible optical absorption measurements (400 to 900 nm) were obtained on a Hewlett-Packard 8453 UV−visible diode array spectrophotometer. Nanowires with width from 45 to 140 nm and a height of 30 nm on BK7 glass substrates were used in the absorption measurements. The polarization of the exciting light was set with a Glan-Thompson polarizer (Newport) to be perpendicular to the long axis of the nanowires.

Optical Diffraction Measurements. Optical diffraction data on Au nanowire arrays were obtained from the LPNE gold nanowire arrays using a 543 nm HeNe laser (Research Electro-Optics, model 30968), a 633 nm HeNe laser (JDS Uniphase, Model 1125p), or an 814 nm diode laser (Melles Griot, model 8902). All of the lasers were chopped at a frequency of 1.0 kHz (EG&G model 650/651). A combination of a Glan-Thompson polarizer (Newport) and a $\lambda/2$ plate (Special Optics) was used to vary the laser power from 1 to 10 mW. Diffraction intensity signal was measured with a Si photodiode detector (Hamamatsu) connected to a DSP lock-in amplifier (EG&G model 7220).

Electrochemistry. Electrochemical measurements were obtained with a three electrode potentiostat (Autolab Model PGSTAT12). The gold nanowires with w = 80 nm, h = 50 nm, and L = 5 mm (active area) were used as working electrode. The electrode potential was referenced to a Ag/AgCl (saturated NaCl) electrode, and a Pt wire was used as counter electrode. Ag was electrodeposited on and stripped from gold nanowires using a 20 μM Ag_2SO_4 + 0.1 M H_2SO_4 aqueous solution by cycling potential between 0.9 and 0.3 V. The area of gold electrode was calculated from the charge of reduction peak after surface oxidation of the gold nanowires in 0.1 M H_2SO_4 aqueous solution, and the charge density due to Ag deposition on gold nanowires was calculated by integration of the cathodic current during Ag^+ reduction.

AUTHOR INFORMATION

Corresponding Author
*E-mail: rcorn@uci.edu.

ACKNOWLEDGMENT

This research was supported by the National Institute of Health (2RO1 GM059622) and the National Science Foundation (CHE-0551935). We would like to thank Aaron R. Halpern for his help in optimization of the nanowire array fabrication methodology and optical diffraction experiments.

REFERENCES

(1) Favier, F.; Walter, E. C.; Zach, M. P.; Benter, T.; Penner, R. M. Hydrogen Sensors and Switches From Electrodeposited Palladium Mesowire Arrays. *Science* **2001**, *293*, 2227–2231.

(2) Murray, B. J.; Li, Q.; Newberg, J. T.; Hemminger, J. C.; Penner, R. M. Silver Oxide (AgxO) Nano- and Microwires: Electrodeposition and Observation of Reversible Resistance Modulation Upon Exposure to Ammonia Vapor. *Chem. Mater.* **2005**, *17*, 6611–6618.

(3) Wan, Q.; Li, Q. H.; Chen, Y. J.; Wang, T. H.; He, X. L.; Li, J. P.; Lin, C. L. Fabrication and Ethanol Sensing Characteristics of ZnO Nanowire Gas Sensors. *Appl. Phys. Lett.* **2004**, *84*, 3654–3656.

(4) Yang, F.; Taggart, D. K.; Penner, R. M. Fast, Sensitive Hydrogen Gas Detection Using Palladium Nanowires that Resist Fracture. *Nano Lett.* **2009**, *9*, 2177–2182.

(5) Patolsky, F.; Zheng, G. F.; Lieber, C. M. Fabrication of Silicon Nanowire Devices for Ultrasensitive, Label-Free, Real-Time Detection of Biological and Chemical Species. *Nat. Protocols* **2006**, *1*, 1711–1724.

(6) He, B.; Morrow, T. J.; Keating, C. D. Nanowire Sensors for Multiplexed Detection of Biomolecules. *Curr. Opin. Chem. Biol.* **2008**, *12*, 522–528.

(7) Cui, Y.; Wei, Q. Q.; Park, H. K.; Lieber, C. M. Nanowire Nanosensors for Highly Sensitive and Selective Detection of Biological and Chemical Species. *Science* **2001**, *293*, 1289–1292.

(8) Menke, E. J.; Thompson, M. A.; Xiang, C. X.; Yang, L. C.; Penner, R. M. Lithographically Patterned Nanowire Electrodeposition. *Nat. Mater.* **2006**, *5*, 914–919.

(9) Xiang, C. X.; Kung, S. C.; Taggart, D. K.; Yang, F.; Thompson, M. A.; Güell, A. G.; Yang, Y. G.; Penner, R. M. Lithographically Patterned Nanowire Electrodeposition: A Method for Patterning Electrically Continuous Metal Nanowires on Dielectrics. *ACS Nano* **2008**, *2*, 1939–1949.

(10) Kung, S. C.; Xing, W.; Donavan, K. C.; Yang, F.; Penner, R. M. Photolithographically Patterned Silver Nanowire Electrodeposition. *Electrochim. Acta* **2010**, *55*, 8074–8080.

(11) Halpern, A. R.; Nishi, N.; Wen, J.; Yang, F.; Xiang, C.; Penner, R. M.; Corn, R. M. Characterization of Electrodeposited Gold and Palladium Nanowire Gratings with Optical Diffraction Measurements. *Anal. Chem.* **2009**, *81*, 5585–5592.

(12) Schider, G.; Krenn, J. R.; Gotschy, W.; Lamprecht, B.; Ditlbacher, H.; Leitner, A.; Aussenegg, F. R. Optical Properties of Ag and Au Nanowire Gratings. *J. Appl. Phys.* **2001**, *90*, 3825–3830.

(13) Lamprecht, B.; Schider, G.; Lechner, R. T.; Ditlbacher, H.; Krenn, J. R.; Leitner, A.; Aussenegg, F. R. Metal Nanoparticle Gratings: Influence of Dipolar Particle Interaction on the Plasmon Resonance. *Phys. Rev. Lett.* **2000**, *84*, 4721–4724.

(14) Chen, H. A.; Lin, H. Y.; Lin, H. N. Localized Surface Plasmon Resonance in Lithographically Fabricated Single Gold Nanowires. *J. Phys. Chem. C* **2010**, *114*, 10359–10364.

(15) Du, L.; Zhang, X.; Mei, T.; Yuan, X. Localized Surface Plasmons, Surface Plasmon Polaritons, and Their Coupling in 2D Metallic Array for SERS. *Opt. Express* **2010**, *18*, 1959–1965.

(16) Kim, F.; Song, J. H.; Yang, P. Photochemical Synthesis of Gold Nanorods. *J. Am. Chem. Soc.* **2002**, *124*, 14316–14317.

(17) Sharma, V.; Park, K.; Srinivasarao, M. Shape Separation of Gold Nanorods Using Centrifugation. *Proc. Natl. Acad. Sci. U.S.A.* **2009**, *106*, 4981–4985.

(18) Rothenhausier, B.; Knoll, W. Total Internal Diffraction of Plasmon Surface Polaritons. *Appl. Phys. Lett.* **1987**, *51*, 783–785.

(19) Tsay, Y. G.; Lin, C. I.; Lee, J.; Gustafson, E. K.; Appelqvist, R.; Magginetti, P.; Norton, R.; Teng, N.; Charlton, D. Optical Biosensor Assay. *Clin. Chem.* **1991**, *37*, 1502–1505.

(20) St. John, P. M.; Davis, R.; Cady, N.; Czajka, J.; Batt, C. A.; Craighead, H. G. Diffraction-Based Cell Detection Using a Microcontact Printed Antibody Grating. *Anal. Chem.* **1998**, *70*, 1108–1111.

(21) Nakajima, F.; Hirakawa, Y.; Kaneta, T.; Imasaka, T. Diffractive Optical Chemical Sensor Based on Light Absorption. *Anal. Chem.* **1999**, *71*, 2262–2265.

(22) Morhard, F.; Pipper, J.; Dahint, R.; Grunze, M. Immobilization of Antibodies in Micropatterns for Cell Detection by Optical Diffraction. *Sens. Actuators, B* **2000**, *70*, 232–242.

(23) Bailey, R. C.; Hupp, J. T. Large-Scale Resonance Amplification of Optical Sensing of Volatile Compounds with Chemoresponsive Visible-Region Diffraction Gratings. *J. Am. Chem. Soc.* **2002**, *124*, 6767–6774.

(24) Bailey, R. C.; Nam, J. M.; Mirkin, C. A.; Hupp, J. T. Real-Time Multicolor DNA Detection with Chemoresponsive Diffraction Gratings and Nanoparticle Probes. *J. Am. Chem. Soc.* **2003**, *125*, 13541–13547.

(25) Yu, F.; Tian, S. J.; Yao, D. F.; Knoll, W. Surface Plasmon Enhanced Diffraction for Label-Free Biosensing. *Anal. Chem.* **2004**, *76*, 3530–3535.

(26) Goh, J. B.; Loo, R. W.; Goh, M. C. Label-Free Monitoring of Multiple Biomolecular Binding Interactions in Real-Time with Diffraction-Based Sensing. *Sens. Actuators, B* **2005**, *106*, 243–248.

(27) Yu, F.; Knoll, W. Surface Plasmon Diffraction Biosensor. *J. Nonlinear Opt. Phys. Mater.* **2005**, *14*, 149–160.
(28) Bornhop, D. J.; Latham, J. C.; Kussrow, A.; Markov, D. A.; Jones, R. D.; Sørensen, H. S. Free-Solution, Label-Free Molecular Interactions Studied by Back-Scattering Interferometry. *Science* **2007**, *317*, 1732–1736.
(29) Wark, A. W.; Qavi, A.; Lee, H. J.; Corn, R. M. Nanoparticle-Enhanced Diffraction Gratings for Ultrasensitive Surface Plasmon Biosensing. *Anal. Chem.* **2007**, *79*, 6697–6701.
(30) Sendroiu, I. E.; Corn, R. M. Nanoparticle Diffraction Gratings for DNA Detection on Photopatterned Glass Substrates. *Biointerphases* **2008**, *3*, FD23–FD29.
(31) Chen, Y.; Kung, S. C.; Taggart, D. K.; Halpern, A. R.; Penner, R. M.; Corn, R. M. Fabricating Nanoscale DNA Patterns with Gold Nanowires. *Anal. Chem.* **2010**, *82*, 3365–3370.
(32) *Handbook of Optical Constants of Solids*; Palik, E. D., Ed.; Academic Press: New York, 1985.